CHEMISTRY OF MATERIALS

pubs.acs.org/cm

Article

Amalgams as Hydrogen-Free Reducing Agents for Topotactic Oxide Deintercalation

Thomas J. Whoriskey,* Gregory Bassen, Brandon Wilfong, Jayson B. Johnson, Daniel C. Naiman, Ari Turkiewicz, Grace A. Pan, Dan Ferenc Segedin, Elizabeth A. Pogue, Julia A. Mundy, and Tyrel M. McQueen*

Cite This: *Chem. Mater.* 2024, 36, 4583−4590

Read Online

ACCESS | Metrics & More | Article Recommendations | Supporting Information

ABSTRACT: Here, we report the development of a hydrogen-free, topotactic oxygen deintercalation technique using alkali metal aluminum gallium amalgams (A_xAlGa, where A = Li, Na, K). These amalgams provide a uniquely tunable system where the choice of alkali metal, its concentration, and the Al:Ga composition alter its reductive properties. We demonstrate the utility of this method in topotactically removing oxygen from bulk and thin film specimens of $LnNiO_3$ (Ln = La, Nd) to form the infinite layer of nickelate $LnNiO_2$ (Ln = La, Nd). For example, $Na_{0.25}AlGa$ affords bulk $LaNiO_2$ from $LaNiO_3$ at 300 °C for 120 h, while the same amalgam at 265 °C for 48 h affords the intermediate $La_2Ni_2O_5$ ($LaNiO_{2.5}$). Other alterations in time and temperature as well as the choice of alkali metal (A) and its concentration (x) in A_xAlGa allow further exploration of the topotactic reduction. Compared to standard techniques based on hydrogen gas or hydrides such as LiH, NaH, and CaH_2, these amalgams offer an elegant tunability of the reduction potential, enabling control over the rate and degree of oxygen removal without the risk of hydrogen intercalation.

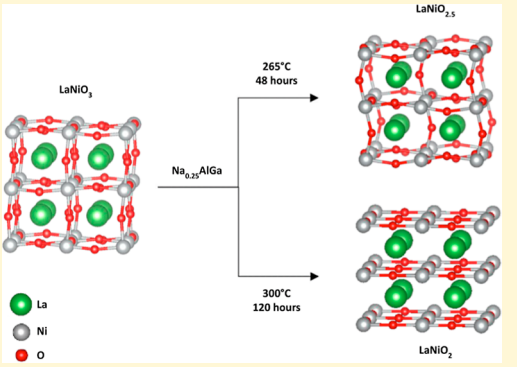

INTRODUCTION

Materials discovery is plagued by the difficulty of retrosynthetically realizing targeted materials, leaving much of the solid-state synthesis as a black box. Unlike the elegant hierarchical synthesis steps common in organic chemistry, solid-state techniques, like high-temperature "shake and bake" methods, hydrothermal synthesis, and flux methods, often lack a priori mechanistic insight, leaving much of synthesis as a blind trial and error process. In more recent years, lower temperature "chimie douce" or soft chemistry topotactic techniques have gained considerable attention as a method to synthesize metastable materials by design through a directed modification process.[1,2] In topotactic chemistry, a precursor material's lattice is treated like a scaffolding to allow for the addition, removal, or rearrangement of targeted atoms.[3−28] In these cases, temperatures are not high enough to destabilize the framework of the chemical structure but instead allow for the diffusion of atoms through a lattice to realize kinetically stabilized products. This kinetically stabilized process can therefore enable a mechanistic approach for solid-state synthesis for the rational design of the desired products. Perovskites and perovskite-like structures have often been of interest for their wide variety of applications including superconductivity, catalysis, and ferroelectrics[29−31] as well as their layered structure showing the ability to be topotactically altered at low temperatures, which has been detailed in previous work.[1]

The most common type of topotactic reactions consists of the intercalation or deintercalation of ionic species, especially in the solid-state battery community. The most famous examples are lithium-ion batteries, where lithium is deintercalated from the host structure, allowing for the remaining lithium ions to diffuse into the empty sites within the layer.[23,24] Moreover, oxygen deintercalation via topotactic reduction has allowed for the discovery of novel families of materials with functional electronic and magnetic applications.[3−9,11−13,15−22] Topotactic modification reveals how small changes in structure, oxidation state, and composition can greatly affect material properties, as seen by the onset of superconductivity upon the intercalation of fluorine in Sr_2CuO_3.[32] Another such example is the discovery of superconductivity in reduced nickelate thin films.[6−11,46]

Nickelates have long been studied due to their interesting properties and as potential analogues to known copper oxide superconductors.[12] The discovery of high-temperature superconductors in copper oxides[33] and later other systems, such as

Received: January 29, 2024
Revised: April 18, 2024
Accepted: April 19, 2024
Published: April 30, 2024

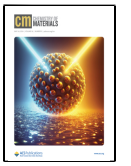

iron-based superconductors,[34] did not fit into the Barden−Cooper−Schrieffer (BCS)[35] theory that explained previously discovered superconductors. The discovery of new families of superconductors expands our understanding of what components are necessary for superconductivity and hopefully will provide deeper insights into the mechanism behind unconventional superconductivity. In particular, recent work has sought to compare nickelate superconductors to high-temperature superconductivity in isoelectronic and isostructural cuprates;[36,37] however, the true extent of overlap between these two families has not yet been fully understood.

In the synthesis of superconducting thin film nickelates, isolation of the infinite layer nickelate requires a topotactic oxygen removal step from the parent perovskite.[6] One reason for the difficulty in reducing $LaNiO_3$ to $LaNiO_2$ is that there exists a narrow temperature regime where the oxygen atoms have sufficient energy to deintercalate from the host lattice while minimizing decomposition of the resulting $LaNiO_2$ phase. However, this generally necessitates the use of hydrogen or hydrides to achieve sufficient reducing potential,[4−6,16−19] complicating inferences about the role of hydrogen in nickelate superconductivity. $LaNiO_2$ was first isolated by Crespin et al.[16] using hydrogen gas; however, the experimental setup was complex and has scarcely been replicated due to its difficulty.[38] The majority of later works utilize other hydrides such as NaH and CaH_2,[4,6,19] which have been used as the preferred low-temperature oxygen deintercalation method, with CaH_2 as the increasingly preferred method due to its higher thermal stability than NaH.[6,19] In 2002, Hayward et al. found that hydrides can intercalate into the lattice forming transition metal oxyhydrides,[25] muddling the effect and role of hydrogen on reduced oxide materials and their properties as more have since been discovered.[10,26−28]

Moreover, Li et al. found that doped and reduced bulk nickelate samples showed an absence of superconductivity as compared to their analogous thin film counterparts.[15] This discrepancy of superconductivity between thin film and bulk nickelates thus far lacks an explanation. Some recent work in currently archived and preprint articles implies that issues with structural defects—including layer buckling—could be inhibiting superconductivity.[39,40] Another prevailing hypothesis is that hydrogen incorporation as a byproduct of the hydride reduction technique affects the electronic properties and, therefore, the presence or absence of superconductivity. Some computational studies and experimental data imply that hydrogen incorporation may be necessary for superconductivity,[10] while some show that this incorporation leads to decreased conductivity.[41−43] SIMS experiments on superconducting nickelates further give contradictory results regarding the significance of hydrogen in these systems.[10,44] Neutron diffraction studies have indicated that there is not a significant amount of hydrogen incorporation in bulk $LaNiO_2$ powder[45] but have not quantified the upper limit of hydrogen present. The presence of strain in thin films could explain the difference in properties between bulk and film samples as well as any differences in the propensity for hydrogen incorporation.

The difficulty in detecting hydrogen in the solid state and the ambiguity of hydrogen's role in nickelate superconductivity motivate the need for a new reduction technique. Some progress in hydride-free reductions has been shown using metals as oxygen getters such as zirconium or aluminum[13,20−22,46] but in bulk samples hydride-free reductions have only resulted in the formation of $LaNiO_{2.5}$ instead of the desired $LaNiO_2$ phase. Thin film samples reduced using aluminum have required an in situ technique that does not easily transfer to bulk samples.[13,46] Aluminum also shows significant reduction potential at low temperatures when mixed with gallium, reacting with water.[47,48] However, as these are extremely powerful reductants, such reactions are very sensitive to precise timing and particle morphology, limiting reaction control and material quality. The conflicting results regarding the role of hydrogen in nickelate superconductivity could be resolved if hydrogen-free samples of reduced nickelates were prepared.

Here, we report a new reduction method for topotactic oxygen deintercalation that utilizes an amalgam of aluminum, gallium, and an alkali metal. The combination of aluminum and gallium provides a "base" considerably less hazardous than mercury conventionally found in amalgams, while the concentration of dissolved alkali metal enables precise control over the reduction potential of the amalgam. This new technique shows promise as an alternative synthetic pathway for oxygen deintercalation, free from many of the conventional pitfalls.

EXPERIMENTAL SECTION

$LaNiO_3$ was prepared using a two-step reaction from a KOH flux.[49] La_2O_3 (Alfa Aesar, 99.99%) and NiO (Strem Chemicals, 99.9%) were preliminarily dried at 1000 and 150 °C, respectively, and stored in a desiccator. The reactants were mixed in a 1:1 ratio and ground into a powder using an agate mortar and pestle and then heated in a box furnace at 1000 °C for 12 h. This powder was then mixed with KOH pellets (Merck) in a ratio of 1:10 by mass, respectively, and heated in a Ni crucible at 450 °C for 12 h. $LaNiO_3$ was also synthesized via a high-pressure floating zone (HPFZ), at 50 bar O_2, as previously described.[50] A section of the melt was crushed into a powder in an agate mortar and pestle for later use. Reductions on these samples kept the entire synthesis process hydrogen-free.

The alkali-free amalgam AlGa was synthesized by placing stoichiometric amounts of aluminum (Kurt J. Lesker, 99.99%) and gallium (Noah Tech, 99.99%) in a carbon-coated quartz tube and heating them in a box furnace at 700 °C for 4 h. All quartz tubes were flushed with argon and sealed under a vacuum of ∼20 mTorr. The product was opened in a glovebox with O_2 < 0.1 ppm and H_2O < 0.5 ppm. The sodium amalgam $Na_{0.25}AlGa$ was prepared by combining Na (Sigma-Aldrich, 99.9% metals basis) with the as-prepared AlGa amalgam in a carbon-coated quartz tube with a Na/Al/Ga ratio of 1:4:4, other stoichiometries, as well as lithium (Sigma-Aldrich, 99% metals basis) and potassium (Sigma-Aldrich, 98% metals basis) analogues prepared by the same procedure. This amalgam was brought to 300 °C for 2 h and then briefly placed in a preheated 700 °C box furnace for approximately 5 min before quenching (to ensure homogeneity of the amalgam). At room temperature, the amalgam consists of small beadlike clusters. All subsequent reductions were prepared in a glovebox by placing the amalgam in direct contact with an ∼50 mg pellet of $LaNiO_3$ (10:1 molar ratio) in a quartz tube. The respective amalgams were ground into a powder to increase the contact surface area between the reducing agents and the nickelate. After heating, the nickelate can be easily separated from the amalgam by mechanically brushing off any amalgam beads from the pellet. Calcium hydride (Alfa Aesar, 92%) reductions, on the other hand, were performed with indirect contact using Al foil as previously described.[11] The furnace was heated to a given temperature at 100 °C/h.

Films were synthesized according to Pan et al.[14] Thin film reductions were performed with the same procedure as the bulk, with 200−300 mg amalgam, compared to ∼1 g for bulk samples. Thin films were oxidized by heating them at 300 °C for 84 h under flowing O_2 at a rate of ∼5 L/h.

https://doi.org/10.1021/acs.chemmater.4c00264
Chem. Mater. 2024, 36, 4583−4590

The following equations were used to determine the 10:1 molar excess for reduction.

$$LaNiO_3 + \left(\frac{2}{3}\right)Al \rightarrow LaNiO_2 + \left(\frac{1}{3}\right)Al_2O_3$$

$$LaNiO_3 + 2A \rightarrow LaNiO_2 + A_2O \qquad (A = Li, Na, K)$$

$$LaNiO_3 + CaH_2 \rightarrow LaNiO_2 + Ca(OH)_2$$

X-ray diffraction (XRD) data were taken using Bruker powder XRD with a Cu Kα anode instrument for bulk samples and a Bruker Four Circle XRD with a Cu Kα anode instrument for thin film samples.

Temperature-dependent magnetic susceptibility data was collected on a Quantum Design Magnetic Property Measurement System (MPMS3) from T = 2−300 K under an applied field of H = 1000 Oe and using zero-field-cooled (ZFC) and field-cooled (FC) protocols. All magnetic data were collected on powder samples loaded with plastic straws. Scanning electron microscopy (SEM) and energy-dispersive spectroscopy (EDS) were performed using a JEOL JSM-IT100 instrument by placing the powder on carbon tape.

Refinements were performed on this data with the use of Topas.[51] We refined the lattice parameters, zero error, background, and the Thompson−Cox−Hastings peak shape.[52] Two background peaks were added at a low angle to account for diffuse scattering present in the spectra due to sample preparation. Structure visualizations were taken from Vesta.[53]

RESULTS AND DISCUSSION

Figure 1 demonstrates the viability of this technique, as applied to the preparation of infinite-layer $LaNiO_2$ from perovskite $LaNiO_3$. It is important to highlight the control of $Na_{0.25}AlGa$ as a reducing agent to convert precursor $LaNiO_3$ to either $LaNiO_{2.5}$ or $LaNiO_2$ as a function of temperature and time.

The parent $LaNiO_3$ compound is a phase-pure hexagonal perovskite crystallizing in $R\bar{3}c$ (167) symmetry as previously reported.[54,55] Reduction of this parent with the gold standard hydride method, CaH_2, produces $LaNiO_2$ at 300 °C with some over-reduced impurity phase (see Figure 1d). There is some impurity phase in the infinite layer phase realized by the sodium amalgam of levels comparable to those of the hydride reduction. Pure Na results in $LaNiO_2$ after 8 h of treatment but results in over-reduction impurity phases as well as significant intermediate phases indicating poor reaction control.

Figure 2 shows a direct comparison between reducing agents, all at 300 °C for 24 h. Only the sodium amalgam and the hydride show significant peaks indicating the $LaNiO_2$ phase after 24 h at 300 °C. The aluminum gallium does not show any significant reductive progress, indicating that it is more of a vessel for controlling the ability of the alkali metal to reduce. Another treatment shown in Figure S1 with just an AlGa mixture, which has previously only shown its reductive capabilities by reducing water,[47,48] does not result in any significant peak shifts or appearance of new phases even after 48 h at 550 °C. This is different than recent findings in thin films, where deposited aluminum layers can reduce $LaNiO_3$ to $LaNiO_2$ as a function of film coverage and temperature (200 to 270 °C).[13] This reflects the differences in required diffusion pathlengths for oxygen deintercalation in thin film and bulk materials: about 50 nm for the thin film case versus micrometers for bulk specimens. However, addition of sodium into the amalgam, nominally $Na_{0.25}AlGa$, allows for a conversion of bulk $LaNiO_3$ to $LaNiO_2$, seen in Figure 1c with sharp peaks indicating strong retention of crystallinity.

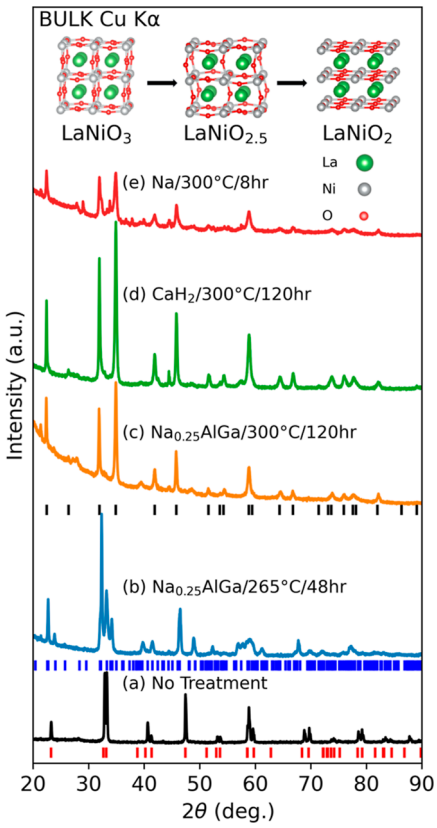

Figure 1. Room temperature powder XRD patterns of $LaNiO_3$ (a) starting material before treatment. (b) Reaction with $Na_{0.25}AlGa$ at 265 °C for 48 h forming $LaNiO_{2.5}$. (c) Reaction with $Na_{0.25}AlGa$ at 300 °C for 120 h forming $LaNiO_2$. (d) Reaction with CaH_2 at 300 °C for 120 h forming $LaNiO_2$. (e) Reaction with Na for 300 °C for 8 h forming $LaNiO_2$. Red tick marks correspond to peak locations for the $LaNiO_3$ phase, blue tick marks correspond to the $LaNiO_{2.5}$ phase, and black tick marks correspond to peak locations for the $LaNiO_2$ phase.

The Li and K amalgams show significant structural changes but only the K amalgam results in the formation of $LaNiO_{2.5}$.

The use of NaAlGa results in over-reduction (Figure S2), demonstrating that the concentration of Na in the amalgam is a key factor controlling the reduction potential and degree of oxygen deintercalation in $LaNiO_3$. One should note that in the case of $LaNiO_3$, the desired reduction potential is obtained with a sodium concentration of $Na_{0.25}AlGa$; however, this may not be the optimal alkali concentration for reductions in other oxide systems. Subsequent fine-tuning of the temperature and reaction time allows us to isolate the intermediate phase $LaNiO_{2.5}$ seen in Figure 1b.

Refinements were performed on various reductions, shown in Figures 3 and S3, with comparisons to the literature values in Table S1. The lattice parameters are compared for the intermediate and infinite layer reduced phases. These strengthen our understanding that the amalgam provides reduction potential comparable to that of CaH_2 while affording better control and crystallinity than sodium alone. Figure S3 expands on the information shown in Figure 3 and includes the hydride reduction refinement. Tick marks in Figure 3 correspond to the intermediate $LaNiO_{2.5}$ and infinite layer $LaNiO_2$ phases, but all the fits and their corresponding weight percent for each sample are presented as well as the R_{wp} values for each Rietveld refinement. The full data are presented in Figure S3. It can be seen that the sodium amalgam allows for

https://doi.org/10.1021/acs.chemmater.4c00264
Chem. Mater. 2024, 36, 4583−4590

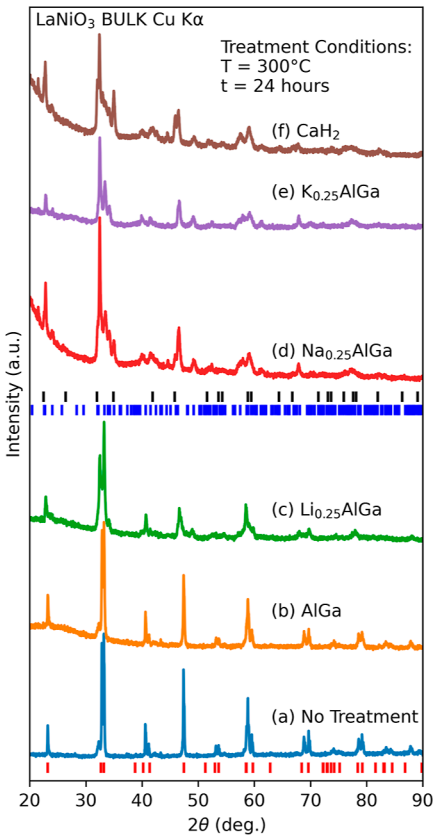

Figure 2. (a) Starting material before treatment (with a small amount of $La_4Ni_3O_{10}$ and unreacted NiO), all subsequent materials in the same furnace at 300 °C for 24 h. (b) Reaction with AlGa; (c) reaction with $Li_{0.25}AlGa$; (d) reaction with $Na_{0.25}AlGa$; (e) reaction with $K_{0.25}AlGa$; and (f) reaction with CaH_2 for 24 h. Red tick marks correspond to peak locations for the $LaNiO_3$ phase, blue tick marks correspond to the $LaNiO_{2.5}$ phase, and black tick marks correspond to peak locations for the $LaNiO_2$ phase.

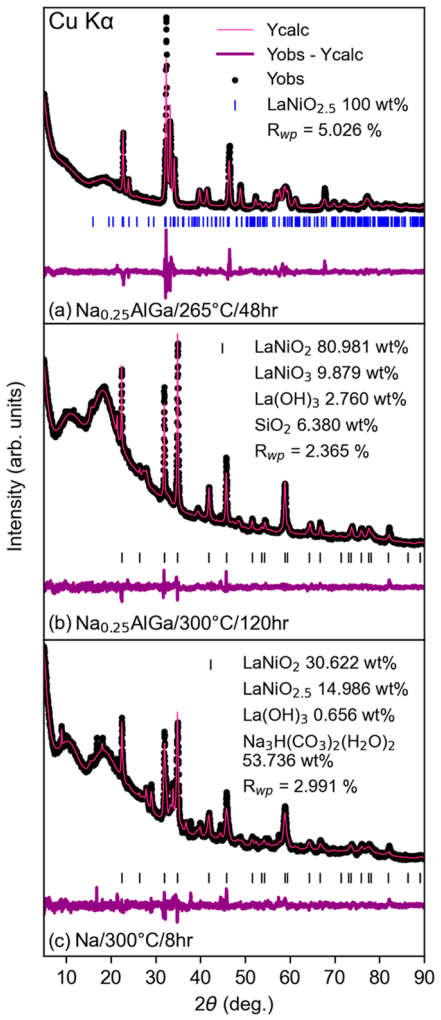

Figure 3. Rietveld refinement for three bulk $LaNiO_3$-reduced samples. (a) Sample reduced by $Na_{0.25}AlGa$ for 48 h at 265 °C forming $LaNiO_{2.5}$; (b) sample reduced for 120 h by $Na_{0.25}AlGa$ at 300 °C forming $LaNiO_2$; and (c) sample reduced for 8 h by Na at 300 °C forming $LaNiO_2$. Black tick marks correspond to peak locations for the $LaNiO_2$ phase, and blue tick marks correspond to peak locations for the $LaNiO_{2.5}$ phase. For each figure, the intermediate $LaNiO_{2.5}$ or infinite layer $LaNiO_2$ is highlighted with peaks, but other phases are presented with their respective weight percent determined by the Rietveld refinement. An expanded version of this figure with all tick marks is presented in SI Figure S3.

the realization of reduced phases of $LaNiO_3$ with little impurity phases, whereas sodium metal alone leads to incomplete reduction and over-reduced phases. It is also estimated that around 50% of the mass of the sample is $Na_3H(CO_3)_2(H_2O)_2$ (likely due to post-synthetic decomposition or reaction in air as there is no available carbon source during the reaction process), making clear the need for other methods than direct reactions with sodium. It should be noted that the larger differences between calculated and observed intensity in Figure 3b are likely due to a combination of incomplete and over-reduced phases. The disagreement in Figure 3c can be attributed to very significant structural changes with small changes in oxygen stoichiometry near the intermediate $LaNiO_{2.5}$ as seen in previous reports.[20,56]

A truly versatile hydrogen-free topotactic oxygen removal method should also be applicable to thin-film specimens in addition to bulk materials. Figure 4 shows the results of applying these amalgams to reduce thin films of $NdNiO_3$ on a $NdGaO_3$ substrate. Reductions via AlGa and $Na_{0.25}AlGa$ were carried out with direct contact between the agent and the film surface.

The CaH_2 reduction was indirectly in contact via Al foil, as described previously,[11] and showed a strong film peak indicating successful oxide deintercalation. The reduction using $Na_{0.25}AlGa$ shows poor crystallinity, but subsequent reoxidation by annealing under flowing oxygen indicates that this is a reversible process and can be fine-tuned for better crystallinity in the future. The XRD pattern for the as-grown film shows intense diffraction peaks for the $NdGaO_3$ substrate and less intense peaks corresponding to the $NdNiO_3$ film. Upon reduction with AlGa, the film peaks shift slightly to a higher angle, suggesting that a small amount of oxygen can be removed. Reduction with $Na_{0.25}AlGa$ and CaH_2 affords the fully reduced phase, evidenced by the dramatic peak shift to a higher angle (Figure 4).

Thin films are generally reduced in indirect contact with hydrides, as diffusion is much more efficient. The amalgam was used in direct contact with the thin film, making oxygen deintercalation difficult to control. Future studies will explore the indirect contact reduction of thin films using the amalgam to optimize the reduction conditions; however, here we

https://doi.org/10.1021/acs.chemmater.4c00264
Chem. Mater. 2024, 36, 4583−4590

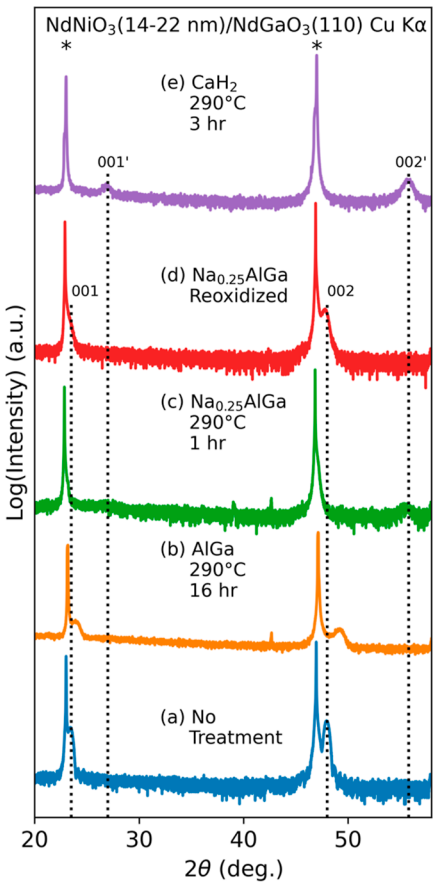

Figure 4. XRD scans of various treatments of $NdNiO_3$ films on $NdGaO_3$, (a) before any reducing treatments. (b) After reaction with AlGa at 290 °C for 16 h, rightward shifted peaks indicate larger structural changes. (c) After reaction with $Na_{0.25}AlGa$ at 290 °C for 1 h. (d) Reduced film shown in (c) after heating with flowing oxygen at 300 °C for 84 h. The reoxidized film shows that this reaction is reversible and therefore nondestructive. (e) After reaction with CaH_2 in indirect contact with film at 290 °C for 3 h. The asterisk denotes the $NdGaO_3$ substrate peaks. The dotted lines represent film peaks.

focused on the bulk samples as a proof of concept that a hydrogen-free reduction method can be implemented. We propose that sodium is the preferred alkali metal for amalgam reductions as it optimizes both kinetic and thermodynamic parameters. Potassium is a larger, more reactive metal than sodium or lithium, making it more difficult to precisely control the reactivity. On the other hand, lithium is smaller, less reactive, and possibly not sufficiently reducing to drive reduction. Therefore, sodium is preferred as its intermediate size allows for maximized diffusivity to reactivity to promote the reduction. The kinetics of the reduction can further be driven by the surface area and size of the starting material, where crystalline materials require longer reduction times compared to their polycrystalline, higher surface area counterparts.

Figures S4−S13 and Tables S2−S11 show various SEM, EDS, magnetic property measurement system (MPMS), and XRD data for precursors and reduced phases. To disambiguate the role of hydrogen in the reduced nickelates, both the hydride and amalgam products were measured on the MPMS, as any hydrogen incorporation would change the number of unpaired spins in the reduced nickelate samples. One can imagine that hydride incorporation would promote $LaNiO_2H_x$ formation and, in the $x = 1$ case, oxidize the nickel from a d^9 to a d^8 with either two unpaired electrons and a higher moment in the high-spin configuration or no unpaired electrons and thus lower moment in the low-spin configuration. Hence, any incorporation of hydrogen should be reflected in the magnetic data. Figures S5 and S8 show the DC susceptibility for the amalgam and hydride-reduced samples, respectively, and show comparable magnetism without significant deviation from one another. It should be noted that part of the high magnetic background is contributed by ferromagnetic reduced nickel metal; however, the literature comparison to $LaNiO_2$ shows similar low-temperature behavior, and shows similar low-temperature behavior as well as ferromagnetic nickel impurity.[6,57] Comparison between the intermediate phase with literature shows comparable magnetic responses.[56] The pure sodium reduction in Figure S7 shows some different magnetic behavior, likely from the other impurity phases present. This suggests that the amount of hydrogen incorporation in bulk samples is small, consistent with the lack of a large incoherent scattering background in neutron powder diffraction.[45] To further test the role of hydrogen in bulk samples and its relationship to superconductivity, samples were hole-doped with strontium and reduced by using the amalgam. Again, we observe no sign of superconductivity in our hydrogen-free reduced powder samples of nominal $La_{0.8}Sr_{0.2}NiO_2$ (Figure S10).

To better understand the nature of the amalgam and its effect on the final product, all precursor and reduced samples were measured with SEM−EDS. Although hydrogen cannot be detected by EDS, a qualitative comparison of the oxygen content can be addressed, along with any contaminants from differing growth conditions. The precursor $LaNiO_3$ samples grown by either the KOH flux or HPFZ did not have significantly different oxygen contents, as shown by Figures S4 and S11 suggestive of comparable oxidizing growth conditions. There are differences in crystallite size and shape due to the different synthesis conditions. This can be seen in the SEM images in Figures S4 and S11. There are many small crystals with a lot of surface area in the 5−10 μm region in S4, whereas the image in Figure S11 shows a crystal with a width on the order of 50 μm. More difficulty isolating the infinite layer phase in floating zone grown samples is consistent with much larger crystal sizes in floating zone samples. The KOH flux did show evidence of small amounts of potassium incorporation on the order of ∼1%, which is consistent with previous work[49] and can be avoided by using the HPFZ or other high oxygen pressure methods. However, the KOH flux was the preferred method for growing $LaNiO_3$ due to the reliability, ease, and scalability of the reaction. The $LaNiO_2$ hydride and amalgam-reduced samples were also measured with EDS. The CaH_2-reduced sample did not show evidence of contaminants, which is expected as the reducing technique involves indirect contact (Figure S8). Although our amalgam technique relies on direct contact with the sample, the reduced products did not show evidence of amalgam incorporation. In fact, the primary contaminants for these sodium amalgam samples were small amounts of potassium, presumably from the KOH flux of precursor $LaNiO_3$, as discussed above. On the other hand, the $LaNiO_2$ sample reduced from pure sodium (without the Al and Ga) showed significant sodium contamination consisting of 11% of the measured sample (Figure S7). As SEM−EDS is a surface technique, one explanation is the post-synthesis

https://doi.org/10.1021/acs.chemmater.4c00264
Chem. Mater. 2024, 36, 4583−4590

workup wherein the amalgam is easier to brush off and remove from the sample than pure sodium.

CONCLUSIONS

In conclusion, we have successfully developed a novel hydrogen-free oxygen deintercalation technique utilizing an amalgam made from aluminum, gallium, and an alkali metal. The reduction capabilities were demonstrated by converting both bulk and thin film nickelates into their infinite layer form. This method marks a distinctive advantage over conventional reducing methods, as changes in alkali concentration allow for a highly tunable reducing system, which helps to moderate both control and degree of oxygen reduction. This is not true of hydride reducing agents, whose reduction potentials are fixed. Moreover, amalgams avoid the risk of hydrogen incorporation into the host lattice, which is often difficult to detect. Therefore, amalgams can be used to disambiguate the role of hydrogen in reduced oxide materials through an alternative synthesis route. In particular, the claim that superconductivity is only found in thin film nickelates with certain amounts of incorporated hydrogen can be experimentally tested by making a hydrogen-free analogue of both thin film and bulk samples.

Overall, amalgams are a highly tunable alternative to hydride reducing agents; the concentration of the reactive ternary metal allows for control over the reduction potential, while the aluminum/gallium ratio controls the melting point. It is clear that the alkali metals are the most important piece of the puzzle when it comes to reducing power, but the sodium reduction alone leaves a lot to be desired in terms of cleanliness and ability to isolate the desired phase, which stresses the importance of the amalgam as a base for controlling these results. Although this work explored the efficacy of amalgams in reducing nickelates, there are many other interesting reduced oxide materials to explore. Accordingly, these amalgams show huge potential for materials discovery as the ternary metal could be varied for the targeted deintercalation of specific anions. For example, calcium has one of the strongest metal affinities for the fluorine atom, and future work involves the selective deintercalation of fluoride anions through a calcium addition to the amalgam.[58] Future research will explore the role of these tunable amalgams in deintercalating other families of anions, such as the selective removal of halide or chalcogenide groups, allowing for new classes of quantum materials to be discovered and serving as a fundamental member of a synthetic chemist's toolbox.

ASSOCIATED CONTENT

Supporting Information

The Supporting Information is available free of charge at https://pubs.acs.org/doi/10.1021/acs.chemmater.4c00264.

Reduction using AlGa on a separate precursor with impurity phases; results of overreduction when using potassium amalgam or a sodium amalgam with a higher sodium concentration; more in-depth figures for the refinements in Figure 3 as well as an additional refinement on a sample reduced using CaH_2; comparison between lattice parameters for experimental and literature values; SEM, XRD, EDS, and DC susceptibility data for the various samples mentioned in the paper; quantitative EDS spectral data for the samples in Figure S4 through S12; SEM, XRD, and EDS data for a sample providing a basis for comparison between the samples synthesized and reduced by various methods (PDF)

AUTHOR INFORMATION

Corresponding Authors

Thomas J. Whoriskey − *Department of Chemistry, The Johns Hopkins University, Baltimore, Maryland 21218, United States; Institute for Quantum Matter, William H. Miller III Department of Physics and Astronomy and Department of Materials Science and Engineering, The Johns Hopkins University, Baltimore, Maryland 21218, United States;* orcid.org/0000-0002-6131-050X; Email: twhoris1@jhu.edu

Tyrel M. McQueen − *Department of Chemistry, The Johns Hopkins University, Baltimore, Maryland 21218, United States; Institute for Quantum Matter, William H. Miller III Department of Physics and Astronomy and Department of Materials Science and Engineering, The Johns Hopkins University, Baltimore, Maryland 21218, United States;* orcid.org/0000-0002-8493-4630; Email: mcqueen@jhu.edu

Authors

Gregory Bassen − *Department of Chemistry, The Johns Hopkins University, Baltimore, Maryland 21218, United States; Institute for Quantum Matter, William H. Miller III Department of Physics and Astronomy and Department of Materials Science and Engineering, The Johns Hopkins University, Baltimore, Maryland 21218, United States*

Brandon Wilfong − *Department of Chemistry, The Johns Hopkins University, Baltimore, Maryland 21218, United States; Institute for Quantum Matter, William H. Miller III Department of Physics and Astronomy and Department of Materials Science and Engineering, The Johns Hopkins University, Baltimore, Maryland 21218, United States*

Jayson B. Johnson − *Department of Chemistry, The Johns Hopkins University, Baltimore, Maryland 21218, United States; Institute for Quantum Matter, William H. Miller III Department of Physics and Astronomy, The Johns Hopkins University, Baltimore, Maryland 21218, United States*

Daniel C. Naiman − *Department of Chemistry, The Johns Hopkins University, Baltimore, Maryland 21218, United States; Institute for Quantum Matter, William H. Miller III Department of Physics and Astronomy and Department of Materials Science and Engineering, The Johns Hopkins University, Baltimore, Maryland 21218, United States*

Ari Turkiewicz − *Department of Physics, Harvard University, Cambridge, Massachusetts 02138, United States;* orcid.org/0000-0001-5729-0289

Grace A. Pan − *Department of Physics, Harvard University, Cambridge, Massachusetts 02138, United States*

Dan Ferenc Segedin − *Department of Physics, Harvard University, Cambridge, Massachusetts 02138, United States*

Elizabeth A. Pogue − *Department of Chemistry, The Johns Hopkins University, Baltimore, Maryland 21218, United States; Institute for Quantum Matter, William H. Miller III Department of Physics and Astronomy, The Johns Hopkins University, Baltimore, Maryland 21218, United States;* Present Address: Research and Exploratory Development Department, Johns Hopkins University Applied Physics Laboratory, 11100 Johns Hopkins Road, Laurel, MD 20723, United States

https://doi.org/10.1021/acs.chemmater.4c00264
Chem. Mater. 2024, 36, 4583−4590

Julia A. Mundy − *Department of Physics, Harvard University, Cambridge, Massachusetts 02138, United States;* orcid.org/0000-0001-8454-0124

Complete contact information is available at: https://pubs.acs.org/10.1021/acs.chemmater.4c00264

Author Contributions

E.A.P. and T.M.M. conceived the use of amalgams for reductions. T.J.W. and T.M.M. provided oversight for the entire project. T.J.W., G.B., B.W., D.C.N., and J.B.J. carried out the bulk synthesis, bulk and thin film reduction experiments, and analysis. A.T., G.P., D.F.S., and J.A.M. prepared the thin film specimens and characterization before reduction and aided in data analysis. All authors helped prepare the manuscript prior to submission.

Funding

This work was funded by the Johns Hopkins University. Thin film synthesis was supported by the US Department of Energy, Office of Basic Energy Sciences, Division of Materials Sciences and Engineering, under award no. DE-SC0021925. The MPMS was funded by the National Science Foundation, USA, Division of Materials Research, Major Research Instrumentation Program, under award 1828490. This work made use of the synthesis facilities of the Platform for the Accelerated Realization, Analysis, and Discovery of Interface Materials (PARADIM), which is supported by the National Science Foundation under Cooperative agreement no. DMR-2039380.

Notes

The authors declare no competing financial interest.

■ ACKNOWLEDGMENTS

The authors acknowledge funding as specified above.

■ REFERENCES

(1) Schaak, R. E.; Mallouk, T. E. Perovskites by Design: A Toolbox of Solid-State Reactions. *Chem. Mater.* **2002**, *14*, 1455−1471.
(2) Chamorro, J. R.; McQueen, T. M. Progress toward Solid State Synthesis by Design. *Acc. Chem. Res.* **2018**, *51*, 2918−2925.
(3) Schaak, R. E.; Mallouk, T. E. Topochemical Synthesis of Three-Dimensional Perovskites from Lamellar Precursors. *J. Am. Chem. Soc.* **2000**, *122* (12), 2798−2803.
(4) Hayward, M. A.; Green, M. A.; Rosseinsky, M. J.; Sloan, J. Sodium Hydride as a Powerful Reducing Agent for Topotactic Oxide Deintercalation: Synthesis and Characterization of the Nickel(I) Oxide $LaNiO_2$. *J. Am. Chem. Soc.* **1999**, *121*, 8843−8854.
(5) Tsujimoto, Y.; Tassel, C.; Hayashi, N.; Watanabe, T.; Kageyama, H.; Yoshimura, K.; Takano, M.; Ceretti, M.; Ritter, C.; Paulus, W. Infinite-layer iron oxide with a square-planar coordination. *Nature* **2007**, *450*, 1062−1065.
(6) Li, D.; Lee, K.; Wang, B. Y.; Osada, M.; Crossley, S.; Lee, H. R.; Cui, Y.; Hikita, Y.; Hwang, H. Y. Superconductivity in an infinite-layer nickelate. *Nature* **2019**, *572*, 624−627.
(7) Pan, G. A.; Ferenc Segedin, D.; LaBollita, H.; Song, Q.; Nica, E. M.; Goodge, B. H.; Pierce, A. T.; Doyle, S.; Novakov, S.; Córdova Carrizales, D.; N'Diaye, A. T.; Shafer, P.; Paik, H.; Heron, J. T.; Mason, J. A.; Yacoby, A.; et al. Superconductivity in a quintuple-layer square-planar nickelate. *Nat. Mater.* **2022**, *21*, 160−164.
(8) Zeng, S.; Li, C.; Chow, L. E.; Cao, Y.; Zhang, Z.; Tang, C. S.; Yin, X.; Lim, Z. S.; Hu, J.; Yang, P.; Ariando, A. Superconductivity in infinite-layer nickelate $La_{1-x}Ca_xNiO_2$ thin films. *Sci. Adv.* **2022**, *8*, No. eabl9927.
(9) Lee, K.; Goodge, B. H.; Li, D.; Osada, M.; Wang, B. Y.; Cui, Y.; Kourkoutis, L. F.; Hwang, H. Y. Aspects of the synthesis of thin film superconducting infinite-layer nickelates. *APL Mater.* **2020**, *8*, 041107.
(10) Ding, X.; Tam, C. C.; Sui, X.; Zhao, Y.; Xu, M.; Choi, J.; Leng, H.; Zhang, J.; Wu, M.; Xiao, H.; Zu, X.; Garcia-Fernandez, M.; Agrestini, S.; Wu, X.; Wang, Q.; Gao, P.; Li, S.; Huang, B.; Zhou, K.; Qiao, L. Critical role of hydrogen for superconductivity in nickelates. *Nature* **2023**, *615*, 50−55.
(11) Ferenc Segedin, D. F.; Goodge, B. H.; Pan, G. A.; Song, Q.; LaBollita, H.; Jung, M.; El-Sherif, H.; Doyle, S.; Turkiewicz, A.; Taylor, N. K.; Mason, J. A.; N'Diaye, A. T.; Paik, H.; Baggari, I. E.; Botana, A. S.; Kourkoutis, L. F.; Brooks, C. M.; Mundy, J. A. Limits to the strain engineering of layered square-planar nickelate thin films. *Nat. Commun.* **2023**, *14*, 1468.
(12) Disa, A. S.; Kumah, D. P.; Ngai, J. H.; Specht, E. D.; Arena, D. A.; Walker, F. J.; Ahn, C. H. Phase diagram of compressively strained nickelate thin films. *APL Mater.* **2013**, *1*, 032110.
(13) Wei, W.; Shin, K.; Hong, H.; Shin, Y.; Thind, A. S.; Yang, Y.; Klie, R. F.; Walker, F. J.; Ahn, C. H. Solid state reduction of nickelate thin films. *Phys. Rev. Mater.* **2023**, *7*, 013802.
(14) Pan, G. A.; Song, Q.; Ferenc Segedin, D.; Jung, M.; El-Sherif, H.; Fleck, E. E.; Goodge, B. H.; Doyle, S.; Córdova Carrizales, D.; N'Diaye, A. T.; Shafer, P.; Paik, H.; Kourkoutis, L. F.; El Baggari, I.; Botana, A. S.; Brooks, C. M.; Mundy, J. A. Synthesis and electronic properties of Ndn+1NinO3n+1 Ruddlesden-Popper nickelate thin films. *Phys. Rev. Mater.* **2022**, *6*, 055003.
(15) Li, Q.; He, C.; Si, J.; Zhu, X.; Zhang, Y.; Wen, H. Absence of superconductivity in bulk Nd1-xSrxNiO2. *Commun. Mater.* **2020**, *1*, 16.
(16) Crespin, M.; Levitz, P.; Gatineau, L. Reduced forms of LaNiO3 perovskite. Part 1.—Evidence for new phases: $La_2Ni_2O_5$ and $LaNiO_2$. *J. Chem. Soc., Faraday Trans.* **1983**, *79*, 1181−1194.
(17) Puphal, P.; Wu, Y.; Fürsich, K.; Lee, H.; Pakdaman, M.; Bruin, J. A. N.; Nuss, J.; Suyolcu, Y. E.; van Aken, P. A.; Keimer, B.; Isobe, M.; Hepting, M. Topotactic transformation of single crystals: From perovskite to infinite-layer nickelates. *Sci. Adv.* **2021**, *7*, 49.
(18) Puphal, P.; Wehinger, B.; Nuss, J.; Küster, K.; Starke, U.; Garbarino, G.; Keimer, B.; Isobe, M.; Hepting, M. Synthesis and physical properties of $LaNiO_2$ crystals. *Phys. Rev. B* **2023**, *7*, 014804.
(19) Takamatsu, T.; Kato, M.; Noji, T.; Koike, Y. Low-temperature synthesis of the infinite-layer compound $LaNiO_2$ using CaH_2 as reductant. *Phys. C* **2010**, *470*, S764−S765.
(20) Moriga, T.; Usaka, O.; Nakabayashi, I.; Kinouchi, T.; Kikkawa, S.; Kanamaru, F. Characterization of oxygen-deficient phases appearing in reduction of the perovskite-type $LaNiO_3$ to $La_2Ni_2O_5$. *Solid State Ionics* **1995**, *79*, 252−255.
(21) Alonso, J. A.; Martinez-Lope, M. J. Preparation and crystal structure of the deficient perovskite $LaNiO_{2.5}$, solved from neutron powder diffraction data. *J. Chem. Soc., Dalton Trans.* **1995**, *17*, 2819−2824.
(22) Hansteen, O. H.; Fjellvåg, H.; Hauback, B. C. Crystal structure, thermal and magnetic properties of La3Co3O8. Phase relations for $LaCoO_{3-\delta}$ ($0.00 \leq \delta \leq 0.50$) at 673 K. *J. Mater. Chem.* **1998**, *8*, 2081−2088.
(23) Kim, T.; Song, W.; Son, D. Y.; Ono, L. K.; Qi, Y. Lithium-ion batteries: outlook on present, future, and hybridized technologies. *J. Mater. Chem. A* **2019**, *7*, 2942−2964.
(24) Whittingham, M. S. Ultimate Limits to intercalation reactions for lithium batteries. *Chem. Rev.* **2014**, *114* (23), 11414−11443.
(25) Hayward, M. A.; Cussen, E. J.; Claridge, J. B.; Bieringer, M.; Rosseinsky, J.; Kiely, C. J.; Blundell, S. J.; Marshall, M.; Pratt, F. L. The Hydride Anion in an Extended Transition Metal Oxide Array: $LaSrCoO_3H_{0.7}$. *Science* **2002**, *295*, 1882−1884.
(26) Masuda, N.; Kobayashi, Y.; Hernandez, O.; Bataille, T.; Paofai, S.; Suzuki, H.; Ritter, C.; Ichijo, N.; Noda, Y.; Takegoshi, K.; Tassel, C.; Yamamoto, T.; Kageyama, H. Hydride in $BaTiO_{2.5}H_{0.5}$: A Labile Ligand in Solid State Chemistry. *J. Am. Chem. Soc.* **2015**, *137* (48), 15315−15321.
(27) Sakaguchi, T.; Kobayashi, Y.; Yajima, T.; Ohkura, M.; Tassel, C.; Takeiri, F.; Mitsuoka, S.; Ohkubo, H.; Yamamoto, T.; Kim, J. E.; Tsuji, N.; Fujihara, A.; Matsushita, Y.; Hester, J.; Avdeev, M.; Ohoyama, K.; Kageyama, H. Oxyhydrides of (Ca,Sr,Ba)TiO_3

Perovskite Solid Solutions. *Inorg. Chem.* **2012**, *51* (21), 11371−11376.
(28) Amano Patino, M.; Zeng, D.; Blundell, S. J.; McGrady, J. E.; Hayward, M. A. Extreme Sensitivity of a Topochemical Reaction to Cation Substitution: $SrVO_2H$ versus SrV_{1-x} $Ti_xO_{1.5}H_{1.5}$. *Inorg. Chem.* **2018**, *57* (5), 2890−2898.
(29) Hazen, R. M. Perovskites. *Sci. Am.* **1988**, *258* (6), 74−80.
(30) Hwang, J.; Rao, R. R.; Giordano, L.; Katayama, Y.; Yu, Y.; Shao-Horn, Y. Perovskites in catalysis and electrocatalysis. *Science* **2017**, *358* (6364), 751−756.
(31) Cohen, R. E. Origin of ferroelectricity in perovskite oxides. *Nature* **1992**, *358*, 136−138.
(32) Ai-Mamouri, M.; Edwards, P. P.; Greaves, C.; Slaski, M. Synthesis and superconducting properties of the strontium copper oxy-fluoride $Sr_2CuO_2F_{2+\delta}$. *Nature* **1994**, *369*, 382−384.
(33) Bednorz, J. G.; Müller, K. A. Z. Possible high Tc superconductivity in the Ba-La-Cu-O system. *Z. Phys. B: Condens. Matter* **1986**, *64*, 189−193.
(34) Kamihara, Y.; Hiramatsu, H.; Hirano, M.; Kawamura, R.; Yanagi, H.; Kamiya, T.; Hosono, H. Iron-Based Layered Superconductor: LaOFeP. *Am. Chem. Soc.* **2006**, *37* (45), 10012−10013.
(35) Bardeen, J.; Cooper, L. N.; Schrieffer, J. R. ″Theory of Superconductivity.″. *Phys. Rev.* **1957**, *108* (5), 1175−1204.
(36) Karp, J.; Botana, A. S.; Norman, M. R.; Park, H.; Zingl, M.; Millis, A. Many-Body Electronic Structure of $NdNiO_2$ and $CaCuO_2$. *Phys. Rev. X* **2020**, *10*, 021061.
(37) Kitatani, M.; Si, L.; Janson, O.; Arita, R.; Zhong, Z.; Held, K. Nickelate superconductors—a renaissance of the one-band Hubbard model. *npj Quantum Mater.* **2020**, *5*, 59.
(38) Lokshin, K. A.; Mitchell, D.; Lobanov, M. V.; Struzhkin, V.; Egami, T. Synthesis and Characterization of Pure Infinite Layer Ni+ Nickelates: $LnNiO_2$ (Ln = La, Nd, Pr) and $La_3Ni_2O_6$" ECS. *J. Solid State Sci. Technol.* **2022**, *11*, 044008.
(39) Song, D.; Hu, K.; Li, Q.; Jia, Y.; Liang, Z.; Du, H.; Wen, H.; Ge, B. Atomic origin of absent superconductivity in bulk infinite-layer nickelate 2023. doi.org/. *Nature Portfolio Preprint*. https://www.researchsquare.com/article/rs-3607723/v1 (accessed April 18, 2024).
(40) Rathnayaka, S.; Yano, S.; Kawashima, K.; Akimitsu, J.; Brown, C. M.; Neuefeind, J.; Louca, D. Layer buckling and absence of superconductivity in $LaNiO_2$. *arXiv* **2024**, arXiv:2403.09826v1.
(41) Si, L.; Worm, P.; Held, K. Fingerprints of Topotactic Hydrogen in Nickelate Superconductors. *Crystals* **2022**, *12*, 656.
(42) Malyi, O. I.; Varignon, J.; Zunger, A. Bulk $NdNiO_2$ is thermodynamically unstable with respect to decomposition while hydrogenation reduces the instability and transforms it from metal to insulator. *Phys. Rev. B* **2022**, *105*, 014106.
(43) Si, L.; Xiao, W.; Kaufmann, J.; Tomczak, J. M.; Lu, Y.; Zhong, Z.; Held, K. Topotactic Hydrogen in Nickelate Superconductors and Akin Infinite-Layer Oxides ABO_2. *Phys. Rev. Lett.* **2020**, *124*, 166402.
(44) Balakrishnan, P. P.; Segeden, D. F.; Chow, L. E.; Quarterman, P.; Muramoto, S.; Surendran, M.; Patel, R. K.; LaBollita, H.; Pan, G. A.; Song, Q.; Zhang, Y.; Baggari, I. E.; Jagadish, K.; Shao, Y.; Goodge, B. H.; Kourkoutis, L. F.; Middey, S.; Botana, A. S.; Ravichandran, J.; Ariando, A.; Mundy, J. A.; Grutter, A. J. Hydrogen is not necessary for superconductivity in topotactically reduced nickelates. *arXiv* **2024**, arXiv:2403.01796v1.
(45) Puphal, P.; Pomjakushin, V.; Ortiz, R. A.; Hammoud, S.; Isobe, M.; Keimer, B.; Hepting, M. Investigation of Hydrogen Incorporations in Bulk Infinite-Layer Nickelates. *Front. Phys.* **2022**, *10*, 842578.
(46) Wei, W.; Vu, D.; Zhang, Z.; Walker, F. J.; Ahn, C. H. Superconducting $Nd_{1-x}Eu_xNiO_2$ thin films using in situ synthesis. *Sci. Adv.* **2023**, *9*, 27.
(47) Kravchenko, O. V.; Semenenko, K. N.; Bulychev, B. M.; Kalmykov, K. B. Activation of aluminum metal and its reaction with water. *J. Alloys Compd.* **2005**, *397*, 58−62.
(48) Jang, S.; Jeghan, S. M. N.; Seon, E.; Tak, Y.; Kim, M.; Lee, G. Unraveling the corrosion kinetics of gallium-aluminum for efficient hydrogen production from water at zero CO_2 emission. *Int. J. Hydrogen Energy* **2023**, *48*, 13390−13403.
(49) Shivakumara, C.; Hegde, M. S.; Prakash, A. S.; Khadar, A. M. A.; Subbanna, G. N.; Lalla, N. P. Low temperature synthesis, structure and properties of alkali-doped La_2NiO_4, $LaNiO_3$ and $LaNi_{0.85}Cu_{0.15}O_3$ from alkali hydroxide fluxes. *Solid State Sci.* **2003**, *5*, 351−357.
(50) Zhang, J.; Zheng, H.; Ren, Y.; Mitchell, J. F. High-Pressure Floating-Zone Growth of Perovskite Nickelate $LaNiO_3$ Single Crystals. *Cryst. Growth Des.* **2017**, *17*, 2730−2735.
(51) Perl, J.; Shin, J.; Schumann, J.; Faddegon, B.; Paganetti, H. TOPAS: an innovative proton Monte Carlo platform for research and clinical applications. *Med. Phys.* **2012**, *39* (11), 6818−6837.
(52) Thompson, P.; Cox, D. E.; Hastings, J. B. Rietveld Refinement of Debye-Scherrer Synchrotron X-ray Data from Al_2O_3. *J. Appl. Crystallogr.* **1987**, *20*, 79−83.
(53) Momma, K.; Izumi, F. ″VESTA 3 for three-dimensional visualization of crystal, volumetric and morphology data,″. *J. Appl. Crystallogr.* **2011**, *44*, 1272−1276.
(54) García-Muñoz, J. L.; Rodríguez-Carvajal, J.; Lacorre, P.; Torrance, J. B. Neutron-diffraction study of*R*NiO3(*R*=La,Pr,Nd,Sm): Electronically induced structural changes across the metal-insulator transition. *Phys. Rev. B* **1992**, *46*, 4414−4425.
(55) Wold, A.; Post, B.; Banks, E. Rare Earth Nickel Oxides. *J. Am. Chem. Soc.* **1957**, *79*, 4911−4913.
(56) Moriga, T.; Usaka, O.; Imamura, T.; Nakabayashi, I.; Matsubara, I.; Kinouchi, T.; Kikkawa, S.; Kanamaru, F. Synthesis, Crystal Structure, and Properties of Oxygen-Deficient Lanthanum Nickelate $LaNiO_{3-x}$ ($0 \le x \le 0.5$). *Bull. Chem. Soc. Jpn.* **1994**, *67* (3), 687−693.
(57) Ortiz, R. A.; Puphal, P.; Klett, M.; Hotz, F.; Kremer, R. K.; Trepka, H.; Hemmida, M.; von Nidda, H. A. K.; Isobe, M.; Khasanov, R.; Luetkens, H.; Hansmann, P.; Keimer, B.; Schafer, T.; Hepting, M. ″Magnetic correlations in infinite-layer nickelates: An experimental and theoretical multimethod study″. *Phys. Rev. Res.* **2022**, *4*, 023093.
(58) Reed, T. B. *Free Energy of Formation of Binary Compounds*; MIT Press: Cambridge, MA, 1971.

https://doi.org/10.1021/acs.chemmater.4c00264
Chem. Mater. 2024, 36, 4583−4590